University of Kentucky

UKnowledge

Theses and Dissertations--Biomedical Engineering

Biomedical Engineering

2014

RELATIONSHIPS OF LONG-TERM BISPHOSPHONATE TREATMENT WITH MEASURES OF BONE MICROARCHITECTURE AND MECHANICAL COMPETENCE

Jonathan Joseph Ward
University of Kentucky, ward12jj@gmail.com

Right click to open a feedback form in a new tab to let us know how this document benefits you.

RELATIONSHIPS OF LONG-TERM BISPHOSPHONATE TREATMENT WITH
MEASURES OF BONE MICROARCHITECTURE AND MECHANICAL
COMPETENCE

THESIS

A thesis submitted in partial fulfillment of the requirements for the degree of Master of
Science in Biomedical Engineering in the College of Engineering at the University of
Kentucky

By

Jonathan Joseph Ward

Lexington, Kentucky

Director: Dr. David Pienkowski, Professor of Biomedical Engineering

Lexington, Kentucky

2014

ABSTRACT OF THESIS

RELATIONSHIPS OF LONG-TERM BISPHOSPHONATE TREATMENT WITH
MEASURES OF BONE MICROARCHITECTURE AND MECHANICAL
COMPETENCE

Oral bisphosphonate drug therapy is a common and effective treatment for osteoporosis. Little is known about the long-term effects of bisphosphonates on bone quality. This study examined the structural and mechanical properties of trabecular bone following 0-16 years of bisphosphonate treatment. Fifty-three iliac crest bone samples of Caucasian women diagnosed with low turnover osteoporosis were identified from the Kentucky Bone Registry. Forty-five were treated with oral bisphosphonates for 1 to 16 years while eight were treatment naive. A section of trabecular bone was chosen from a micro-computed tomography (Scanco μCT 40) scan of each sample for a uniaxial linearly elastic compression simulation using finite element analysis (ANSYS 14.0). Morphometric parameters (BV/TV, SMI, Tb.Sp., etc.) were computed using μCT. Apparent modulus, effective modulus and estimated failure stress were calculated. Biomechanical and morphometric parameters improved with treatment duration, peaked around 7 years, and then declined independently of age. The findings suggest a limit to the benefits associated with bisphosphonate treatment and that extended continuous bisphosphonate treatment does not continue to improve bone quality. Bone quality, and subsequently bone strength, may eventually regress to a state poorer than at the onset of treatment. Treatment duration limited to less than 7 years is recommended.

KEYWORDS: bisphosphonates, bone microarchitecture, finite element analysis, micro-computed tomography, osteoporosis

_____Jonathan Joseph Ward_____

_____November 17, 2014_____

RELATIONSHIPS OF LONG-TERM BISPHOSPHONATE TREATMENT WITH
MEASURES OF BONE MICROARCHITECTURE AND MECHANICAL
COMPETENCE

By

Jonathan Joseph Ward

_____David Pienkowski_____
Director of Thesis

_____Abhijit Patwardhan_____
Director of Graduate Studies

_____November 17, 2014_____

ACKNOWLEDGMENTS

TABLE OF CONTENTS

LIST OF TABLES

LIST OF FIGURES

Introduction

The primary purpose of bone is to act as a storage site for calcium as part of the overall regulation of plasma calcium in the human body. Structural support follows as a secondary purpose. This dual purpose is reflected in the hierarchical structure of bone. At the nanoscale level, all bone consists of mineralized collagen fibrils. The fibrils consist of an organic matrix (30% of volume), which is 90% type I collagen, and mineral nanoparticles made of carbonated hydroxyapatite (70% of volume) [1]. The organization at scales above this depends on the type of bone. At the macroscale level, bone is classified into two types, cortical and cancellous bone (Figure 1). Cortical bone is dense, accounting for approximately 80% of the skeleton's bone mass and contributes mainly to the loadbearing structural purpose of bone. The collagen fibrils are arranged into larger fibers that make up units called osteons in cortical bone at the microscale level. These units are called trabeculae in cancellous bone. In contrast to cortical bone, cancellous bone, also known as "spongy bone" or "trabecular bone", is a porous structure of rods and plates and contributes 10 times as much surface area as cortical bone does [2]. The increased surface area allows trabecular bone to be the primary interface for calcium storage and regulation with the rest of the body.

Ninety-nine percent of the body's calcium, 85% of the phosphate, and 50% of the magnesium are stored in bone [2]. The storage of these minerals contributes to accomplishing both bone's primary purpose of calcium homeostasis as well as the secondary purpose of structural support. The mineral content increases the rigidity and brittleness of the bone [3, 4]. Thus, variations in the tissue of bone at the nanoscale level change the material properties which contribute to overall mechanic response of bone to loading.

Variations in the macroscale and microscale structure of bone greatly influence the biomechanics of bone and are an important factor governing bone quality as well. As previously noted, much of the structural support of bone is contributed by cortical bone; however, the trabecular network also plays a vital role in distributing loads between

1

sections of cortical bone or articulating surfaces [5]. The trabecular network is able to optimize the transmission of loads through changes in key structural parameters. For example, the trabecular struts could change in number, thickness, or shape becoming more plate-like instead of rod-like. Additionally, the fibers forming the osteons or trabeculae are arranged along stress lines so that the bone is more capable of bearing loads in the direction at which those loads are normally experienced [2]. The adaptation of bone structure in response to changes in mechanical loading is a principle known as Wolff's Law.

Adaptations in accordance with Wolff's Law are achieved through bone turnover. Bone turnover is the process by which bone constantly remodels and repairs its structure. Resorption is the first step of bone turnover and is executed by large multinucleated cells called osteoclasts. Osteoclasts work in the shape of a cutting cone secreting hydrogen ions to dissolve the mineral crystals and hydrolytic enzymes to digest the osteoid matrix. The osteoclasts have a linear resorption rate of approximately 50 microns per day [6]. In the next step, bone formation, cells called osteoblasts lay the foundation for new bone by creating the bone collagen matrix. Once the matrix is laid, the bone can undergo mineralization, and calcium is stored. At only approximately 1 micron per day, the linear rate of bone formation is not nearly as fast as the resorption [6].

In normal healthy adults, bone resorption and formation are balanced so that there is no net change in bone mass during the remodeling process. Occasionally, an imbalance in favor of formation will cause a net increase in bone mass such as during human development [7]. Conversely, the disease osteoporosis is characterized by an imbalance between resorption and formation causing a net decrease in bone mass. As a result, the structural integrity of the skeletal system is compromised predisposing the bone to fracture. The majority of these fractures occur at the hip, spine, or forearm. Osteoporotic fractures often lead to a decrease in quality of life for the patient, and fractures of the hip and spine are strongly associated with high mortality within the 2 years following the fracture[8-10]. The World Health Organization (WHO) defines osteoporosis as a bone mineral density (BMD) measurement 2.5 standard deviations or more below the mean

[11]. BMD assessment by dual x-ray absorptiometry (DXA) is the current gold standard for diagnosis [12]. New diagnostic tools such as fracture-risk assessment (FRAX) have been added to the diagnosis process because osteoporosis is a disease of low bone strength and not just low bone mass [13, 14].

Unfortunately, osteoporosis is the most prevalent metabolic bone disease in the world and is considered an epidemic in most developed countries [15, 16]. According to the National Osteoporosis Foundation, about 54 million Americans have osteoporosis [17]. Although osteoporosis has been observed in all populations, the disease is most prevalent in women [18]. Natural bone loss with age and decreases in estrogen levels increase the risk of developing osteoporosis. Postmenopausal Caucasian women, therefore, are one of the most at risk populations. Studies report the lifetime risk of fracture, including but not limited to those linked to osteoporosis, for Caucasian women over the age of 50 to be between 40-47.3% [19-21]. These fractures generate a significant socioeconomic burden. In 1990, the worldwide direct and indirect annual cost of hip fractures was estimated to be $35 billion [22]. By 2005, the cost of osteoporotic fractures in the United States alone had reached an estimated $19 billion [1]. This number is expected to continue to increase to $25.3 billion by 2025 [17].

Lifestyle modifications such as increased weight-bearing exercise and smoking cessation along with calcium and vitamin D supplementation are recommended as a baseline treatment. In addition, drug therapies are often necessary to treat osteoporosis [19]. Efforts to combat the turnover imbalance associated with osteoporosis fall into two classes, anabolic and antiresorptive therapies. Two osteoanabolic drugs, parathyroid hormone (PTH) and teriparatide, are currently available. These drugs increase bone formation by targeting the signaling pathways to the osteoclasts and osteoblasts [23]. Denosumab, an antiresorptive, targets the signaling pathway to osteoclasts leading to reduced bone resorption [23].

Currently, bisphosphonates are the oldest and most popular of the antiresorptive drugs approved for the treatment of osteoporosis. The primary mechanism of action is the

reduction of turnover by binding to bone hydroxyapatite and inducing apoptosis of osteoclasts [24] (Figure 2). Bone turnover has been shown to decrease up to 90% with bisphosphonates [25]. As the age of the bone tissue increases, BMD and mineral homogeneity also increase. Ultimately, this leads to an increased resistance to fracture. Numerous studies have documented a reduced risk of osteoporotic fractures associated with bisphosphonates [26-29].

Understanding how bisphosphonates help prevent fracture involves studying how osteoporosis and bisphosphonates alter all aspects of bone quality. In addition to mineralization and turnover, bone quality encompasses bone architecture, geometry, tissue properties, and microdamage (Figure 3). Each of these factors can be evaluated using a variety of tests and tools [30]. Infrared spectroscopy was used to show that 3 years of bisphosphonate treatment was associated with increased mineral content while having no significant effect on other tissue properties such as crystallinity or collagen maturity [31]. Microdamage in dogs was found to increase with 3 years of bisphosphonate treatment, but the microdamage was not significantly greater than the levels found after 1 year of treatment [32]. Several studies have documented the preservation of bone microarchitecture through 3 years of bisphosphonate treatment using various imaging technologies [33-37].

While the benefits of bisphosphonates for bone strength in the short-term are well documented and undisputed, evidence that these benefits continue with long-term treatment is sparse. It has been shown that gains in BMD and a drop in bone turnover rate over the first 5 years of treatment are preserved through 10 years of treatment [38]. BMD and bone turnover measures, however, do not completely explain bone mechanical competency. Furthermore, concerns have arisen over atypical fractures of the femur observed in patients undergoing long-term bisphosphonate therapy [39, 40]. The exact cause of these fractures has yet to be determined. Such concerns associated with long-term bisphosphonate treatment have caused some to suggest that a "drug holiday" may be necessary, and consideration is growing for a stoppage in bisphosphonate treatment after

3-5 years [41, 42]. More evidence is required before any official recommendations can be made.

Recent improvements in imaging technology have allowed for greater clarity in the examination of bone microarchitecture. Peripheral quantitative computed tomography (pQCT) has been used in the clinical setting to assess bone density and architecture. Typical resolutions are in the range of ~80 to 100 μm. It has been suggested, however, that scans at this range of resolution may not provide reliable structural detail [43]. Micro-computed tomography (μCT; microCT) is able to capture 3D images with a resolution as low as 8 μm. These high resolution scans of bone biopsies allow for both a visual and quantitative assessment of trabecular microarchitecture. Studies have confirmed the ability of microCT to provide 3D morphometric data with accuracy and in less time than conventional histomorphometry [44-46].

Overall bone mechanics can be analyzed through mechanical testing such as a uniaxial compression test of a trabecular bone segment. By physically loading an actual segment of bone, the test accounts for nearly all the factors contributing to bone's resistance to fracture intrinsic to the bone segment, but a biopsy is required and will be destroyed in the process. As an alternative, finite element analysis (FEA) is an engineering tool initially developed for the aerospace industry that is capable of simulating mechanical testing. The method consists of discretizing the object of study into a finite number of pieces or elements. Relevant material properties are assigned to the elements, and desired boundary conditions such as a force or displacement are applied. Equations of static or dynamic equilibrium associated with each element are computed until a solution is reached for the unknown variables.

FEA provides a visualization of bone's mechanical competency and insight into the contribution of bone material properties and architecture. Initially, FEA studies of trabecular bone analyzed idealized models consisting of a combination of plates and beams meant to mimic trabecular geometry [47]. As with any simulation, FEA is only as accurate as the input for the simulation. The introduction of 3D digital reconstructions of

bone segments allowed for accurate representation of actual bone architecture in finite element models [5]. The methods for converting image-based models into FEA meshes and for applying boundary conditions continue to be refined in order to ensure that the mechanical analyses accurately represent the state of the bone [48-50].

The behavior of trabecular bone in the elastic region has been shown to fit a linear model [51]. The slope of the linear relationship between load force and displacement in this region is the bone's stiffness. Similarly, the slope of the linear relationship between stress and strain is the bone's Young's modulus of elasticity which is a measure of rigidity. Mechanical properties of trabecular bone in the elastic region such as stiffness and Young's modulus of elasticity have been shown to be strong predictors of bone strength [52, 53]. Many FEA studies of trabecular bone segments, therefore, conduct a linear analysis to assess overall bone strength [37, 48, 54, 55]. Methods for capturing the nonlinear behavior in the plastic region of deformation continue to be developed and refined [56]. Numerous studies have verified that FEA can accurately reproduce the results of mechanical tests where a bone segment is physically crushed [48, 53, 54, 56]. The evolution of FEA in the study of trabecular bone mechanics and the current state of the art have recently been detailed [57].

Previous studies have raised questions and concerns over the efficacy of long-term use of the commonly prescribed bisphosphonates. Currently, few studies examining the effects of bisphosphonates on bone quantity and quality extend beyond 5 years of treatment. Furthermore, studies spanning a longer treatment duration focus primarily on just bone quantity. To broaden the understanding on this subject, this study aimed to 1) quantify the relationship of bisphosphonate treatment of varying durations with the mechanical competency of bone and 2) to assess the relationships between microCT-derived structural indices and FEA-derived biomechanical measures. Consequently, this study tested the hypothesis that there is a relationship between long-term bisphosphonate treatment and measures of bone mechanics and bone microarchitecture.
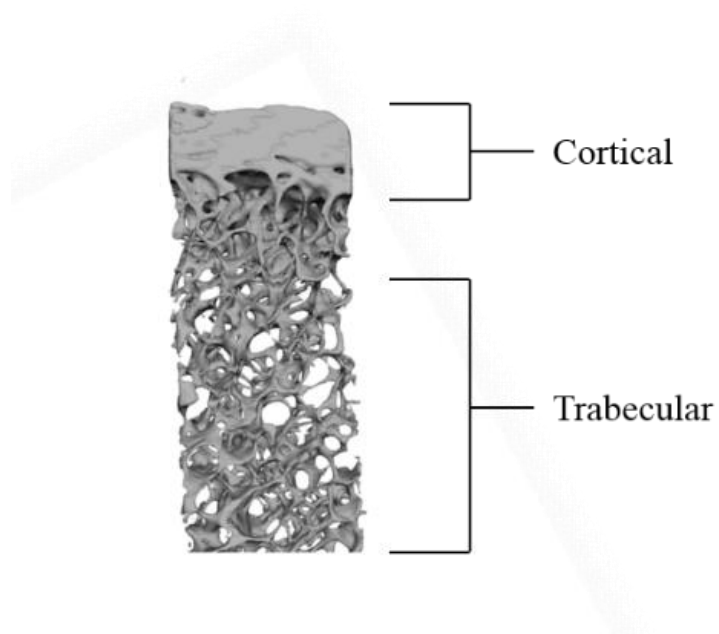
Figure 1. Cortical and trabecular bone.
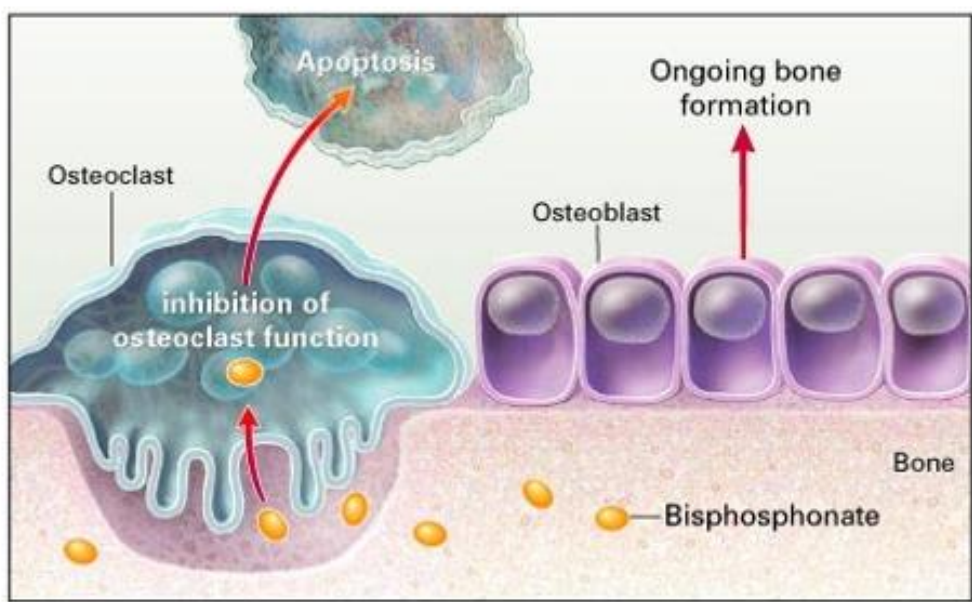
Figure 2. Proposed bisphosphonate mechanism of action. Reproduced with permission from Solomon, CG. Bisphosphonates and osteoporosis. *N Engl J Med.*2002, 346:642., Copyright Massachusetts Medical Society.
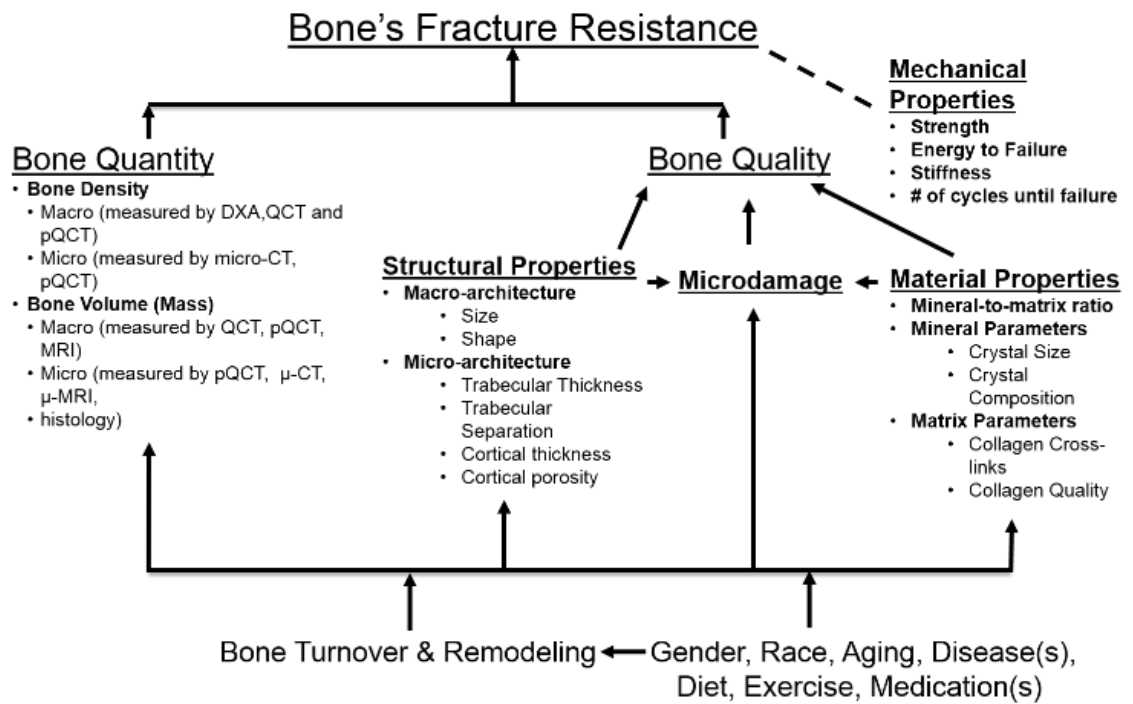
Figure 3. Factors determining the quality and fracture resistance of bone.

Methods

Study Design

      This computer-based study examined trabecular bone from postmenopausal women diagnosed with osteoporosis to determine the relationships among bisphosphonate treatment of widely varying (0-16 years) duration, microarchitecture and mechanical properties. Analysis was limited to trabecular bone as the technique used to procure the biopsies did not consistently provide a segment of cortical bone suitable for study. Power calculations of a previous study [58] indicated that a sample size of 50 spread evenly over 15 years of treatment along with 10 untreated specimens was required to detect a change in strength with treatment duration (power = 0.95, α = 0.05).

      Structural indices to be measured from microCT-based 3D morphometry included:

1. bone volume fraction (BV/TV)
2. structure model index (SMI)
3. connectivity density (CD)
4. trabecular separation (Tb.Sp.)
5. trabecular thickness (Tb.Th.)

Biomechanical properties to be calculated from linearly elastic FEA included:

1. apparent modulus (E_{app})
2. effective modulus (E_{eff})
3. estimated failure stress (P_{fail})

Bone Sample Procurement

      Much of the focus of the FEA study of human trabecular bone has been conducted using bone from the vertebrae of cadavers. The Kentucky Bone Registry's vast database of bone biopsies obtained from the iliac crest offered an opportunity for an unprecedented study of bone from living subjects with varying durations of bisphosphonate treatment. Approximately 8,000 biopsies have been collected in the available database. All biopsies were obtained for diagnostic purposes by sterile, minimally invasive surgical procedures performed at the University of Kentucky Medical Center. All bone biopsies were extracted by drilling into the superior surface of the subject's anterior iliac crest. The

resulting cores were either 3 mm or 4 mm in diameter. Cores were then "fixed with ethanol at room temperature, dehydrated, and embedded in methylmethacrylate" [59] (Figure 4).

Subject Inclusion Criteria

Alendronate (Fosamax) became the first bisphosphonate to receive FDA approval for the treatment of osteoporosis in September 1995. The other two oral bisphosphonates included in the present study, risedronate (Actonel) and ibandronate (Boniva), were approved in 1999 and 2003, respectively. For this reason, no biopsies obtained prior to 1995 were included in the present study. Furthermore, due to improvements in the available clinical notes starting in 1998, only the 1649 biopsies extracted from 1998 to 2013 were of interest (Figure 5). Biopsies were selected from this subset according to strict criteria based on the subject's medical history. Based on the corresponding clinic notes, 434 biopsies were from Caucasian female subjects at least 35 years of age who were diagnosed with low turnover osteoporosis (Figure 5). Low bone turnover was diagnosed by qualitative assessment of the biopsy histology slide. Since bisphosphonates are known to suppress turnover, the presence of high turnover would suggest an abnormal response or a compliance issue with the prescribed drug regimen. Hence, biopsies that displayed high turnover were more likely to be associated with poor compliance.

Subject Exclusion Criteria

Subjects were excluded if the clinic notes indicated prior treatment with long-term steroids, anticonvulsants found to influence bone loss (e.g. phenobarbital), or other osteoporosis drug therapies (e.g. teriparatide or denosumab). Diagnosis of other bone diseases (e.g. Paget's disease or Osteogenesis imperfecta) and any other abnormal conditions (e.g. recent cancer or paraplegia) were also a cause for exclusion. After all medical exclusion criteria were applied, 211 subjects remained (Figure 5).

Biopsies from these subjects were then checked for poor biopsy quality. To assess overall quality, biopsies which met the medical criteria were initially examined under a microscope (Leica StereoZoom, Leica Microsystems, Heerbrugg, Switzerland) at 2.5x magnification for physical criteria. An eligible biopsy for study must have demonstrated

at least a 4mm long straight segment of trabecular bone free from the influence of cortical bone. Ideally, the biopsies would be at least 3-5mm in diameter or, more specifically, spanning at least 5 intratrabecular lengths in each direction to satisfy the continuum assumption [60]. The continuum assumption means that the bone segment can be assumed to be an accurate representation of the state of bone throughout the body. Unfortunately, this would be far too limiting for the study as all biopsies were extracted as nominally 4-mm diameter cores (prior to 2006) or 3-mm diameter cores (2006-Present).

Preferably, the embedded biopsy would be obtained for analysis prior to cutting for histology. If the biopsy had been cut, the depth of the biopsy perpendicular to the cutting plane was measured with a digital micrometer (Marathon, Richmond Hill, Canada; resolution: 0.001mm, accuracy: 0.002mm). This depth measurement was an estimate due to the imprecision associated with measuring an embedded biopsy (Figure 6). Biopsies with an estimated depth reduced to under 2.000 mm were immediately excluded. After this initial check of biopsy quality, biopsies from 97 subjects remained eligible (Figure 5).

MicroCT Scanning

Biopsies that met both the medical history and the physical quality criteria were enrolled in the study. Analysis of these samples began by scanning each biopsy using a Scanco μCT40 (Scanco AG, Zurich, Switzerland) to obtain a digital reproduction of the bone. Briefly, microtomography works by means of a source and a detector on either side of the tested object. A small tube that emits a fan-beam of x-rays at a small angle acts as the source and a linear CCD-array acts as the detector. As the x-ray beam penetrates the object, the denser the material is, the more radiation is absorbed. Before reaching the CCD-array, the x-rays are transformed into visible light by a scintillator. This process of acquiring absorption information is repeated as the object is rotated 180° while the source and detector remain fixed. The data collected at each projection along the rotation is compiled into a sinogram which plots the data using coordinates of the projection angle and the distance along the projection [61]. The image is reconstructed by means of a standard convolution procedure [62]. The result is a single 2D slice of the object. In order

to obtain a 3D image, the whole process is repeated moving in specified increments along the object's axis of rotation until the desired number of slices is acquired.

Scanning Procedure

The scanning procedure started with the creation of an appropriate control file. All biopsies were scanned using the same control file settings of 70 kV energy, 114 µA intensity, 500 projections per 180°, and 30 µm voxel size. The voxel size was dictated by the number of projections and the 30.7-mm field of view; this was the minimum size required to capture the full diameter of the tube used to hold the biopsy. A 0.5-mm aluminum filter was also applied to reduce the effect of beam hardening which would reduce the quality of the segmentation [63]. Scanco provided holders in various sizes, and the 30-mm diameter tube was the smallest that could hold the PMMA cylinders in which the biopsies were embedded. Once the control file was created, a single biopsy was packed tightly into its holder with foam, and securely placed in the scanner. Any motion of the biopsy other than the controlled rotation could significantly reduce the quality of the scan.

A scout scan was completed for each biopsy yielding a preview image which was used to identify the number of slices necessary to capture the entire biopsy. More slices equated to a longer scan time. Therefore, the minimum number of slices required to capture the entire biopsy was desired. This number varied with each biopsy and depended on both the size of the biopsy and the angle at which it was embedded in the PMMA cylinder. Generally, the number of slices was between 70-150 slices which corresponded to a scanning time of 9-20 minutes per biopsy with roughly the same amount of time required for image reconstruction. The scout view also provided a more accurate measurement of the depth of the biopsy, thus samples could drop out at this stage if this value was deemed less than 2.05 mm. Upon selection of the number of slices, the full scan commenced.

2D Inspection

Once scanning finished, the biopsy was opened for 2D analysis where each slice of the scan could be analyzed (Figure 7). In these images, the differences between cortical and trabecular bone were more distinct. Thus, this step also served as a second check of the quality inspection previously completed with the microscope. Each slice was coarsely contoured to define the volume of interest for the creation of a 3D segment. At this stage, the volume of interest included the entire biopsy.

3D Segmentation

A 3D segment was created after the voxels describing bone were distinguished from the background voxels within the volume of interest. This involved taking each image containing pixels along a grayscale continuum and declaring each as either black (background) or white (bone). A Gaussian filter with a sigma of 1.2 and support of 1.0 was applied to reduce noise [62]. The threshold at which voxels were considered bone had to be chosen carefully to ensure that the 3D segment accurately represents the amount of bone and architecture of the bone. Following Scanco's recommendations, a single global threshold value was applied to all samples in the study.

This value for the appropriate global threshold was determined by the "gold standard" procedure of using an external method to verify the correct bone volume of the specimen [64]. In this case, analysis of histology slides served as the external method. Seven biopsies were found to have a μCT slice that matched one of the biopsy's histology slides. The histological bone volume was found by defining the bone area under 20x magnification (Axioplan 2 Imaging, Carl Zeiss, Thornwood, NY), and bone volume measurements were provided by the accompanying histomorphometry software (OsteoMeasureXP 3.0, OsteoMetrics, Inc., Decatur, GA). For each biopsy, μCT-based 2D histomorphometry was completed multiple times using a different threshold value each time until the μCT-based bone volume matched the bone volume of the corresponding histology slice. The mean threshold value at which this occurred for the seven biopsies was 146 (units of 1/1000). This value was designated as the appropriate global threshold for the study.

Three biopsies in the study, however, were scanned with a density calibration applied. This is known to change the threshold value and therefore, required a different global threshold value. Using density-calibrated scans of the same seven biopsies as before, the same procedure of matching the bone volume to the corresponding histology slice was followed resulting in a threshold value of 214 for the density-calibrated biopsies. The resulting 3D segments were saved on the hard drive as a seg.aim files.

Using the Scanco Image Processing Language (IPL) code, a surface tessellation language (STL) file was created from the seg.aim file for each biopsy. STL files are a commonly used format in CAD manufacturing and rapid prototyping to transfer geometry data. As part of this process, the surface of the 3D segment was smoothed as the bricklike voxels were triangulated into the surface mesh of the STL file. Upon creation, each STL file was transferred to the computer on which the FEA was run.

Preprocessing of 3D Bone Models
Once downloaded, the 3D model underwent a stage of preprocessing using Netfabb Basic (Netfabb GmbH, Lupburg, Germany). Netfabb provides a range of software products for use in 3D printing and additive manufacturing. Of their products, Netfabb Basic offers the lowest range of capabilities yet is freely distributed and met all study requirements. The program was used to reorient the cylindrical bone models so that the axis of loading was normal to the circular end face of the tested segment (Figure 8). Each virtual specimen was rotated along the x, y, and z axes until the alignment appeared correct from multiple points of view. For a more quantitative assessment, the correct alignment generally coincided with the minimum values for the x, y, and z dimensions. Angles of rotation were recorded. A 4 mm segment measured along the axis of loading was digitally cut from the middle of the straightest portion of trabecular bone. Aside from providing the desired segment length, cutting a portion from the middle of the virtual bone model ensured that both ends of the segment were flat in the plane normal to the axis of loading which was desired for both consistency and convenience in applying the boundary conditions of the FEA.

The preprocessing in Netfabb also served as a final check of the physical quality of the bone segment. The bone segment was aligned so that the shortest dimension of the segment corresponded to the biopsy depth estimated previously. The measure of the shortest dimension was recorded (minimum dimension). Fifty-five biopsies remained for FEA after samples were excluded for either insufficient trabecular bone, excessive processing, excessive influence of subcortical bone, or excessive bending or tapering.

The last step within Netfabb involved an automatic repair of the STL geometry. Digitally cutting out the 4 mm segment often created holes in the surface mesh of the segment which was of primary concern as any holes would prevent the creation of a solid mesh. All biopsies underwent the automatic repair as a precaution. Nonmanifold edges, removal of double triangles and duplicate vertices were among the problems corrected as part of the automatic repair as well. A repair tolerance of 2 microns was acceptable as this fell well below the resolution of the microCT scan. The bone segments were now ready for mesh creation.

Mesh Creation

The STL mesh was just a shell defining the geometry; therefore, the creation of a volume mesh based on the STL was necessary to run a structural analysis. ANSYS ICEM CFD 14.5 (ANSYS® Academic Research, Release 14.5) was the program chosen to create the mesh. Mesh creation and refinement is an important step within the finite element method for determining how accurately the model will represent the response to the applied boundary conditions. After the STL file was imported into the program, ICEM was used to generate the mesh following user-defined settings. Although many bone FEA studies used hexahedral "brick" elements converted directly from the voxels, this study used tetrahedral elements. The reason for this difference was twofold: 1) preprocessing required the transition to an STL which smoothed the voxels into a triangulated shell making a direct conversion to brick elements impossible, and 2) while tending to be artificially stiffer compared to hexagonal elements, the tetrahedral elements could more accurately represent the complexity of the geometry.

The Octree Method was the algorithm chosen for automatic creation of the tetrahedral mesh. This method was first developed in the 1980's and worked by enclosing the entire geometry in a uniform tetrahedral mesh. The large elements were then subdivided into smaller elements until the desired resolution and constraints were achieved. Following conformation of the elements to the geometry surfaces, elements outside of the geometry were removed. Mesh smoothing by moving and merging nodes and deletion of poor elements finished the method.

Automatic Mesh Creation Settings

Previously, a convergence study was conducted to determine the appropriate settings for the automatic mesh creation [58]. In general, a smaller and thus, a greater number of elements would result in more accurate results. However, more elements also would require more equations that must be solved which could progress to a computation requirement beyond the available software and hardware capabilities. The goal of the convergence study was to find the parameter values that would provide reasonably accurate results with the least computational cost. The focus was chiefly on adjusting the global maximum element size, the minimum element size, the edge criterion, and mesh coarsening.

The global maximum element size defines the seed element size that produces a uniform mesh. To satisfy the computation requirements of the Octree method, the defined value should be a factor of 2. The rest of the parameters under scrutiny fall under the process of mesh refinement. Mesh refinement acknowledges that especially in a complex geometry, certain locations will experience greater variations in stress over others and will, therefore, require a finer mesh to accurately describe these variations. For example, a sharp corner will experience an abrupt rise in stress requiring a much finer mesh in comparison to a uniform flat surface. The minimum element size defines the limit for how small an element can be as the mesh refinement attempts to capture curvatures in the geometry. The edge criterion is a value from 0 to 1 that defines how exact sharp edges of the geometry will be represented with values approaching 0 being the most exact. Reducing this value increases mesh refinement but may also lead to the creation of

elements of poor quality (i.e., extremely acute angles). Coarsening the mesh is a final step of enlarging unnecessarily small elements where possible in the interior of the model to reduce the number of elements without affecting the mesh's ability to capture features. A limit on the allowable aspect ratio restrains how much coarsening occurs.

As a result of the convergence study, the global maximum element size was set at 0.250 mm. Also included in the global mesh parameters, the scale factor was set at 1 since the geometry from the imported STL file was automatically in the actual dimensions of the bone segment. Curvature/proximity based refinement was enabled to optimize computational cost. This parameter allows for the use of smaller elements to more accurately capture local curvatures but also limits the cost by defining a minimum element size. The minimum size limit of 0.050 mm resulted from the convergence study. As previously stated, a mesh type of tetrahedral elements created using the Octree Method was set within the volume meshing parameters. Also within the volume parameters, the optimal edge criterion was determined to be 0.050 by the convergence study. Preserving the default settings, the smooth mesh option was enabled and set to run five iterations with a minimum quality of 0.4 as a constraint. Per the convergence study, the coarsen mesh option was enabled to reduce element number over two iterations with a worst aspect ratio of 0.2 as a limit. All parameters were automatically fixed to their settings using a script file.

Mesh Quality Inspection
Once the settings were finalized, the creation and refinement of the mesh commenced. The process took approximately 5 minutes per biopsy to complete. A quality check was then necessary before proceeding. Upon creation of the mesh, all connected elements were considered to be a single material. Free-floating elements had to be deleted for all elements in the analysis to be properly constrained. These elements arose from various stages of the process including inability of the mesh to capture extremely small connections, connections lost as the segment was cut in Netfabb, and free-floating pieces of bone embedded in the PMMA block. Fortunately, they were easily removed once the primary material was identified; all other mesh materials were selected and deleted.

A further visual inspection as well as a quantitative assessment of the mesh quality was conducted on the remaining volume mesh (Figure 9). Mesh quality was assessed numerically based on element aspect ratios and angle idealization [50]. The aspect ratio quantifies how close the shape of the element is to the ideal. The values range from 0 to 1 with 1 representing the ideal tetrahedral element with equilateral sides. Poor quality was defined as an element with an aspect ratio less than 0.33. Only one biopsy had a mesh containing greater than the recommended 5% of elements considered poor at 5.61%. The mean percentage of poor elements by aspect ratio was 2.58%. Quality was also assessed with the criterion of maximum dihedral angle. The acceptable range for dihedral angles was between 30° and 150° [65]. The mean percentage of poor quality elements by maximum dihedral angle was 0.01% with all meshes falling well below the recommended 5% threshold. Once the mesh was verified, an ANSYS .in file was created to import the mesh into ANSYS Mechanical APDL. Of particular note in running this command, the mesh for analysis included only the volume elements and no bar or shell elements.

Finite Element Analysis

Finite element analysis of the models was conducted using APDL code for a batch analysis in ANSYS Mechanical (ANSYS® Academic Research, Release 14.5). This commonly used software was chosen for its availability within the laboratory, ease of use, and vast range of capabilities including nonlinear analyses, optimization studies, buckling, and drop-out of failed elements. The code for an automated batch analysis was previously developed [58]. A simulated 1% strain compression test was chosen as the mode of analysis. Numerous studies have verified that compression simulations using FEA accurately reproduce the results of mechanical compression tests where a bone segment is physically crushed [48, 53, 54, 56]. For all the models, solid 4 node brick (solid185) elements were used and were defined by the imported mesh .in file.

Assignment of Material Properties

Once the elements were defined, material properties were assigned. Each finite element model consisted of a single material whose properties were considered to be

isotropic, linear elastic, and uniform with a Poisson ratio of 0.3 and a Young's modulus of 16.0 GPa. Although bone is an anisotropic material, the assumption of isotropic material properties was shown to be reasonable and significantly simplifies the analysis because of the complexity of the trabecular geometry. The value for Young's modulus for the tissue fell within the range of reported values for trabecular bone [66].

Application of Boundary Conditions

Defining the test conditions was the next step after the model properties were set. Boundary conditions were applied fixing the displacement and rotation to zero for the nodes at the bottom 5% of the model to prevent rigid body motion. Nodes in the top 5% were subjected to a displacement of 1% compressive strain in the y-direction while the remaining displacements and rotations were fixed at zero (Figure 10). The constraints were similar to a mechanical compression test using end caps. Because of the boundary conditions, only the middle 90% of each bone segment contained useful information regarding the reaction stresses.

FEA Output

Output of the FEA included the volume of the elements in the model (Bone Volume), the bone segment length (Length) and the total reaction force along the axis of loading. Additionally, an estimate of the force required to induce failure was calculated during the post-processing within ANSYS. Overall segment failure could be assumed when 2% of the stressed bone volume reached an equivalent strain of 0.7% [54]. The force required to meet this criteria was recorded in the output as the ultimate force. Further visual assessment of the response of the bone segment to the loading conditions was conducted through the creation of contour plots (Figure 11). These plots revealed where the bone segment was weakest.

CT-based Histomorphometry

Gathering 3D histomorphometry data was required before all calculations could be completed. Using the previously recorded angles from the realignment in Netfabb, the microCT images were realigned and reconstructed to simplify defining the volume of interest specific to the 4mm section. The approximate location of the 4mm segment was

based on the distance between the topmost point of the entire biopsy volume and the top of the 4mm segment as well as the angle of the rotation into the slices of the scan (offset angle). To save time, refinement of the contouring which defined the area of interest was limited to the approximate location of the 4mm segment along with an extra 2mm at each end (Figure 7). Because the offset angle could not be corrected, the region of interest for 3D evaluation had an oversized length of 136 voxels (4.08mm) and was centered on the 4mm segment used for FEA. The same values previously applied to the 3D segmentation parameters (i.e., global threshold, Gaussian sigma and support) were used again. A 3D visualization of the region of interest in Scanco's 3D evaluation window was compared to the segment in Netfabb in order to ensure that the same location was analyzed. Relevant results included the total volume (μCT TV), connectivity density (CD), structure model index (SMI), trabecular thickness (Tb.Th.), and trabecular separation (Tb.Sp.). SMI is a quantification of the trabecular structure with zero representing a more plate-like structure and three representing a more rod-like structure. All reported values were calculated without the assumption of a plate model.

Post-Processing

The cross-sectional area used to determine stress and modulus values was calculated by dividing the microCT-based total volume of interest by the length of the volume of interest while taking into account the offset angle.

$$Area = \frac{\mu CT\ TV}{\mu CT\ Length * 0.030/\cos(offset)}$$

The ratio of bone volume to total volume (BV/TV) of each 4mm segment was calculated using the volume of the mesh elements and the product of the cross-sectional area and segment length.

$$BV/TV = \frac{BV}{Area * Length}$$

Apparent Young's modulus was defined as the reaction stress divided by the strain boundary condition and is a measure of the rigidity of the entire tissue volume. Another modulus value, the effective Young's modulus, normalized the apparent Young's modulus to the BV/TV thus providing insight into how efficiently the structure made use of available material. Finally, the estimated failure stress was determined by dividing the ultimate force by the cross-sectional area and provided an estimation of the stress at which failure of the segment would occur.

The apparent modulus, effective modulus, and failure stress were multiplied by a correction factor to account for the effect of lost connections in the trabecular network around the periphery of the segment [67]. These sources of error are known as side artifacts. The outer perimeter with a thickness of approximately half the trabecular separation is a region where load-bearing capacity is likely compromised due to side artifacts. The correction factor was calculated as a ratio of the measured cross-sectional area to the true cross-sectional area defined as just the inner core where the load-bearing capacity was not compromised.

Statistical Analyses

All resulting data was subjected to statistical analyses using SAS 9.3 (SAS Institute Inc., Cary, North Carolina). General linear regression models (PROC GLM in SAS) were used to first relate the biomechanical response variables (e.g. apparent modulus, effective modulus, and predicted failure stress) to duration of bisphosphonate treatment, specimen cross-sectional area, and subject characteristics such as age. Effect of treatment duration was modeled using polynomial regression. Fit of the models were tested using residual variability among subjects with the same treatment duration and adjusted for covariates. The microCT-derived structural response variables (e.g. BV/TV, SMI, CD, Tb.Th., and Tb.Sp.) were also related to these independent variables. Finally, polynomial regression models were used to relate the biomechanical response variables to the microCT-derived structural indices to determine which indices were the most significant predictors of the biomechanical properties. A $p<0.05$ was considered statistically significant.

Three assumptions are made in linear regression models: 1) the response variables are best described as a linear function of the independent variables, 2) the error terms are independent of each other, and 3) for any value of the independent variables, the corresponding value of the response variable is normally distributed with equal variance about the mean response for all values of the independent variables [68]. Plots of the response variables vs. the independent variables with the prediction equations superimposed were generated to examine the fit of the models. The Kolmogorov-Smirnov test was conducted to check the assumption of normality and homogeneity of errors. In case of failure to meet this assumption, an appropriate transformation was applied.

Figure 4. Biopsy embedded in PMMA.
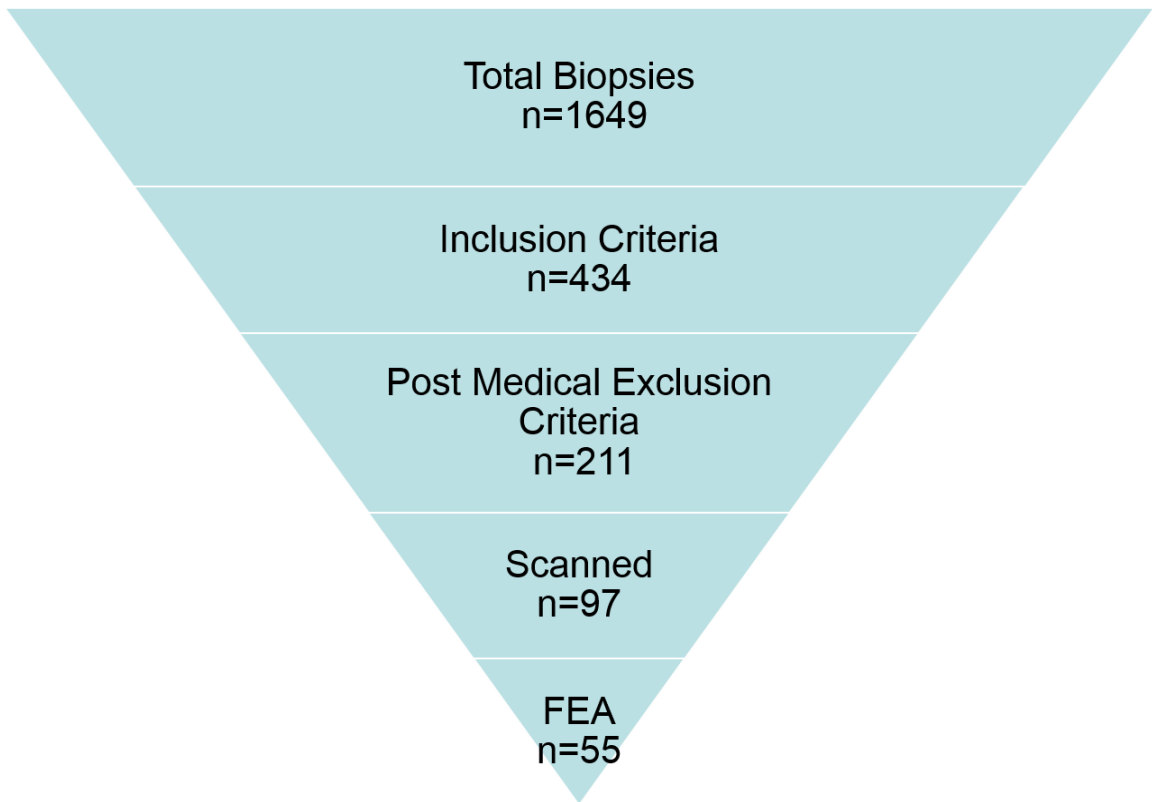
Figure 5. Progression of sample eligibility.

Figure 6. Initial check of biopsy depth.
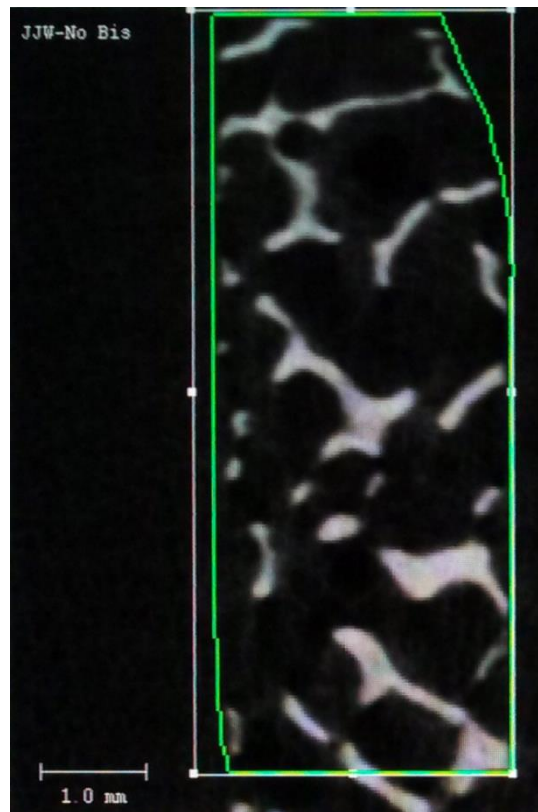
Figure 7. MicroCT slice with contour
lines (green) indicating the volume of
interest.
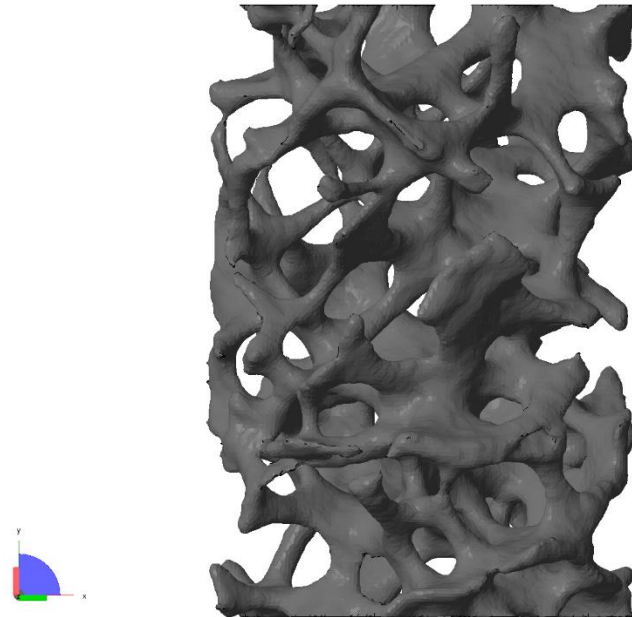
Figure 8. 3D bone model rotated, cut to a 4mm length, and repaired in Netfabb Basic.

Figure 9. Tetrahedral mesh of a 3D bone model generated in ANSYS ICEM CFD.
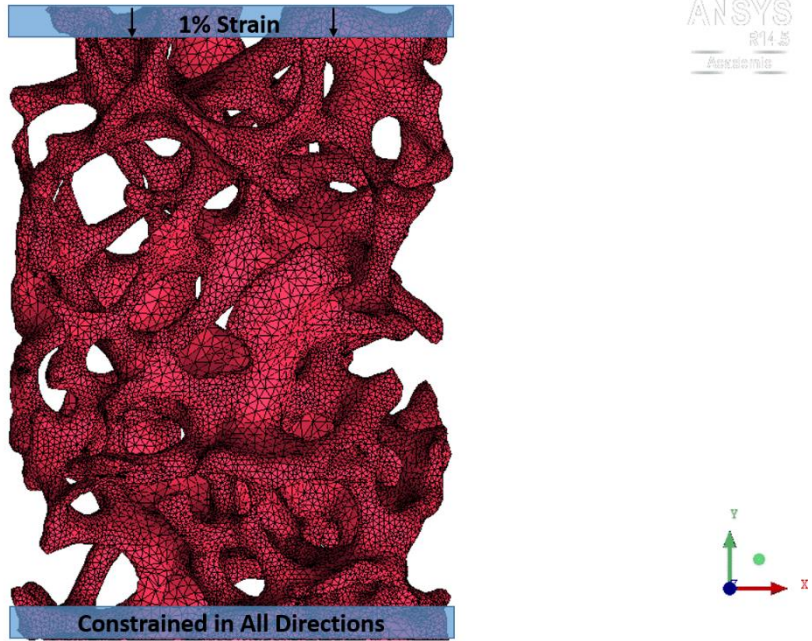
Figure 10. Boundary conditions applied to the ends of the specimen.
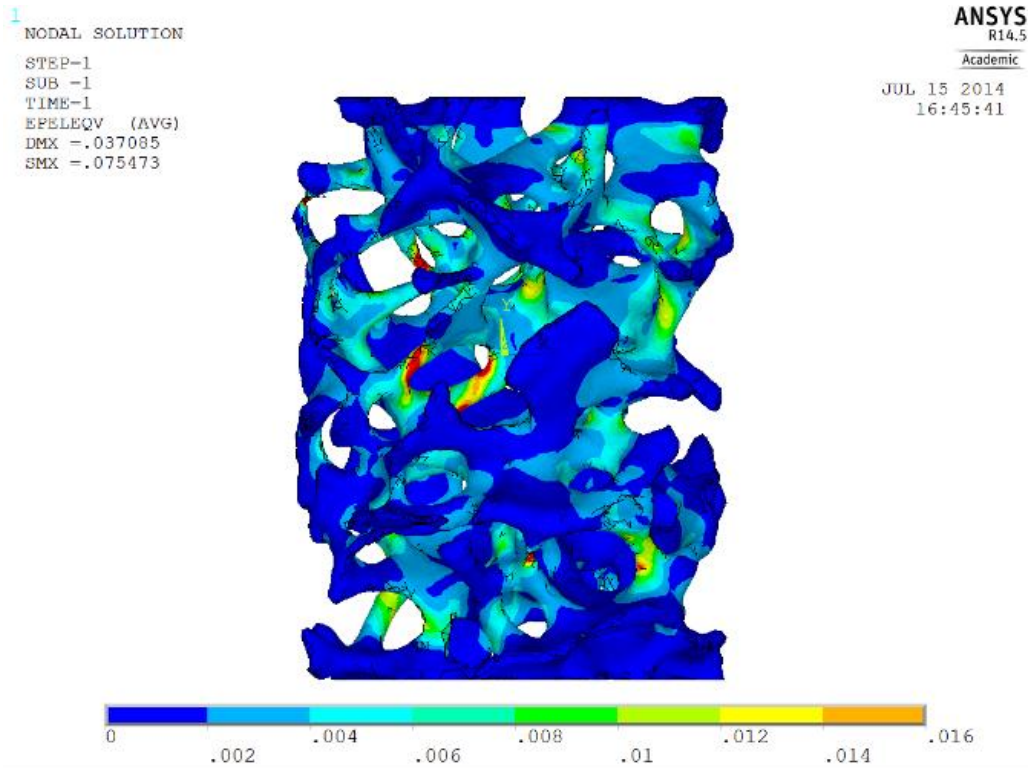
Figure 11. Visual assessment of the load distribution throughout the bone segment from FEA with red indicating the weakest locations.

Results

Fifty-three subjects were included in the analysis after two were excluded. One subject was excluded due to abnormal loading conditions caused by large voids at the constrained ends of the bone segment. Another was excluded after investigation of the subject's medical history revealed bisphosphonate treatment began at age 32.

Average cross-sectional area was not found to have a significant contribution to the prediction of any of the response variables when adjusted for age and treatment duration. These variables included apparent modulus, effective modulus, failure stress, bone volume fraction (BV/TV), structure model index (SMI), connectivity density (CD), trabecular thickness (Tb.Th.), and trabecular separation (Tb.Sp.). Therefore, cross-sectional area was removed from the regression models. Heterogeneity in the response variables at different treatment durations was revealed by the Kolmogorov-Smirnov tests. Square root transformations were applied to all of the response variables to resolve the heterogeneity.

Apparent modulus was significantly predicted by age and a linear and quadratic term for duration of treatment (Table 1). The prediction equation for apparent modulus increased, reached a maximum at a treatment duration of 7.16 ± 0.67 years (Constance Wood, personal communication, July 21, 2014), and then decreased (Figure 12a).

Similar results were obtained with the effective modulus and estimated failure stress as functions of age and duration of treatment (Table 1). The prediction equation for effective modulus increased, reached a maximum at a treatment duration of 7.07 ± 0.65 years (Constance Wood, personal communication, July 21, 2014), and then decreased (Figure 12b). The prediction equation for failure stress increased, reached a maximum at a treatment duration of 7.06 ± 0.64 years (Constance Wood, personal communication, July 21, 2014), and then decreased (Figure 12c).

All of the reported structural indices except for trabecular thickness were significantly predicted by age and a linear and quadratic term for treatment duration

(Table 1). The prediction equations for BV/TV (Figure 12d) and connectivity density (CD, Figure 13a) increased, reached a maximum, and then decreased. The maximum occurred at 6.88 ± 0.69 years for BV/TV and at 6.84 ± 0.98 years for CD (Constance Wood, personal communication, July 21, 2014). The prediction equations for SMI (Figure 13b) and Tb.Sp. (Figure 13c) decreased, reached a minimum, and then increased. The minimum occurred at 6.58 ± 0.87 years for SMI and at 6.83 ± 0.96 years for Tb.Sp (Constance Wood, personal communication, July 21, 2014).

Individually, all the microCT-derived structural indices were significant predictors of the FEA-derived biomechanical properties (Table 2). BV/TV (Figure 14a) and SMI (Figure 14b) were the strongest predictors of apparent modulus, effective modulus, and failure stress. In addition, the analysis was completed with all the structural indices included as independent variables in the regression model. In this case, only BV/TV and SMI significantly contributed to the prediction of the biomechanical variables. Together, microCT-derived BV/TV and SMI were able to explain 81.5% of apparent modulus, 60.4% of the effective modulus, and 86.1% of the failure stress (Table 2).

Table 1. Linear Regression Correlation Coefficients of FEA and MicroCT Measurements Regressed on Age and Duration of Bisphosphonate Treatment

Response Variable	Intercept	Age	Duration	Duration^2	Vertex	R^2
E_{app}	1.326	-0.015	0.117	-0.008	7.16	0.325
E_{eff}	2.832	-0.027*	0.241	-0.017	7.07	0.311
P_{fail}	3.265	-0.032	0.239	-0.017	7.06	0.347
BV/TV	0.579	-0.004	0.023	-0.002	6.88	0.382
SMI	1.061	0.007*	-0.050	0.004	6.58	0.230
Tb.Sp.	19.753	0.111	-0.474*	0.035	6.83	0.299
CD	3.099	-0.021*	0.121*	-0.009*	6.84	0.218

Note:*$p<0.05$. $p<0.01$ for all unmarked coefficients.
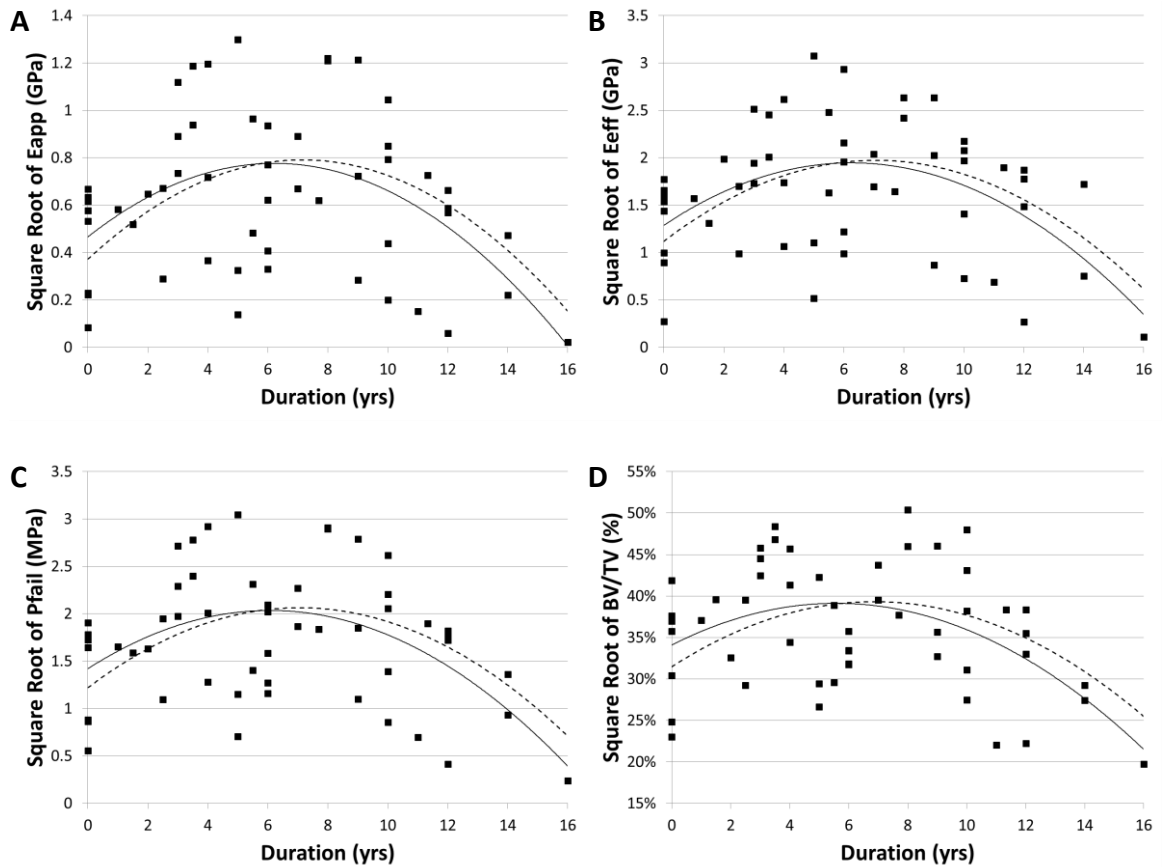
Figure 12. Relationships between bisphosphonate treatment duration and (a) apparent modulus, (b) effective modulus, (c) failure stress, and (d) bone volume fraction. The solid trendlines are fitted to the raw data; the dotted trendlines are fitted to subject age(63 years)-adjusted data.
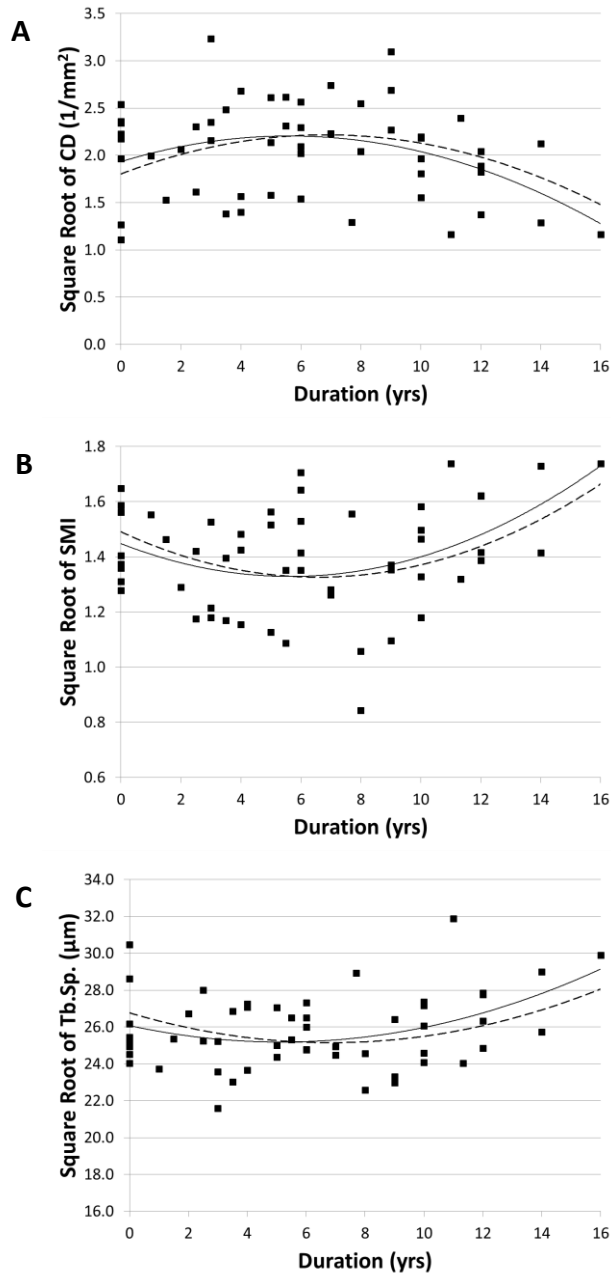
Figure 13. Relationships between bisphosphonate treatment duration and (a) connectivity density, (b) structure model index, and (c) trabecular separation. The solid trendlines are fitted to the raw data; the dotted trendlines are fitted to subject age(63 years)-adjusted data.

Table 2. Linear Regression R^2 Values of FEA Measurements Regressed on MicroCT Measurements

Independent Variable(s)	E_{app}	E_{eff}	P_{fail}
BV/TV	0.782	0.542	0.831
SMI	0.606	0.507	0.626
Tb.Sp.	0.259	0.195	0.263
CD	0.163	0.150	0.156
Tb.Th	0.230	0.134	0.266
BV/TV and SMI	0.816	0.604	0.861

Note: p<0.01 for all models.
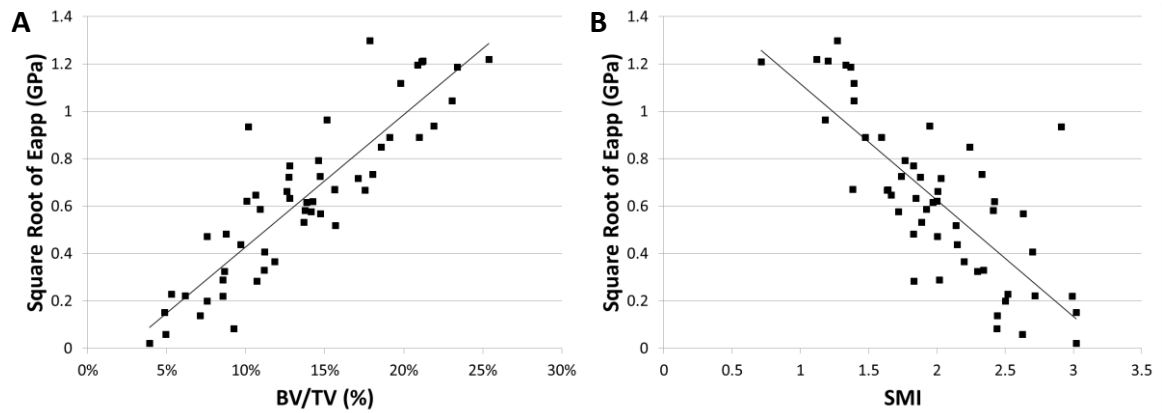
Figure 14. Linear correlations of (a) Bone volume fraction and (b) SMI with apparent modulus.

Discussion

The key findings of this study were the following:

1. The duration of bisphosphonate treatment was significantly related to trabecular bone microarchitecture and the calculated mechanical properties of trabecular bone.

2. The initial positive associations of bisphosphonate treatment with bone microarchitecture and with the calculated mechanical properties of trabecular bone were observed through approximately 6-7 years of continuous treatment.

3. Beyond approximately 6-7 years, the relationships between bisphosphonate treatment and bone microarchitecture and mechanical properties were no longer positive.

4. Moreover, the average values per year of treatment for bone microarchitecture and mechanical properties began to decline. At extremely long durations, these properties were potentially worse than the values of these parameters for untreated bone.

5. BV/TV and SMI were significant predictors of the calculated mechanical properties of trabecular bone and contributed significant information independent of each other.

This study provides novel insight into the effects of long-term bisphosphonate treatment on trabecular microarchitecture. Previous studies have examined the relationships between treatment duration and the structural indices. In studies of up to 3 years of treatment, bisphosphonates have been shown to at least preserve microarchitecture with trends toward an increase in BV/TV and a decrease in trabecular separation [33-35]. Furthermore, a previous study incorporating FEA has reported an increase in trabecular strength after a year of ibandronate [36]. Another study noted an increase in stiffness and failure load in the tibia after 2 years of bisphosphonates, although the change from baseline was not significant [37]. These studies support the initial positive outcomes linked to bisphosphonates. However, the treatment durations of

these studies were too short to comment on the negative trends associated with longer durations of treatment.

Little was previously known about the effects of long-term bisphosphonate treatment on bone quality other than its relationships with BMD and turnover [38]. While studies of BMD have supported the assumption of continued efficacy [29, 38], concerns have arisen over reports of atypical femoral fractures occurring during bisphosphonate treatment with a greater prevalence linked to long-term duration of treatment [40, 42, 69, 70]. This study provided valuable information regarding the correlations between long-term bisphosphonate treatment and measures of bone quantity and bone microarchitecture, a key component of bone quality.

The prediction equations of this study noted a parabolic relationship between the structural state of trabecular bone and long durations of bisphosphonate treatment. The duration of treatment range at which the average mechanical competency decreased, above approximately 7 years, was similar to the duration of treatment ranges where incidence rates of atypical fractures have been reported to be highest [69, 70]. In the present study, the calculated biomechanical properties based on the structure and volume fraction alone were no worse for subjects at 11 years of treatment than for those at 3 years. Studies reported an increase in atypical fracture rates with duration of treatment [69, 70]. The largest increase in the age-adjusted atypical fracture rate occurred going from the 6.0-7.9 years of treatment grouping to the 8.0-9.9 years of treatment grouping [69]. This suggests that while a decline in bone quantity and microarchitecture likely contributed to the prevalence of atypical fractures, aspects of bone quality not analyzed in the present study may be effected by longer treatment durations in a way that compromises bone strength.

It is important to stress that the correlations reported between bisphosphonate treatment and the calculated biomechanical properties and microCT-derived structural indices were independent of the previously reported influence of specimen size and age on bone specimen mechanical properties [71]. The size of the bone specimens used were

smaller in comparison to many other FEA studies of trabecular bone. However, no significant independent effects of bone cross-sectional area on the any of the response variables were reported. Age was significantly correlated to a decline in bone microarchitecture and mechanical properties, but the correlations found with age and the correlations found with treatment were independent of each other. Therefore, the declines in bone quantity, microarchitecture, and mechanical properties observed with long-term treatment cannot be attributed to the effects of aging.

Increase in subject age corresponded to poor bone quality based on all of the structural indices examined including BV/TV, SMI, CD, Tb.Th., and Tb.Sp. This agrees with numerous reports of declines in bone structure with age as demonstrated by a negative correlation with BV/TV, Tb.Th., and CD and a positive correlation with Tb.Sp. and SMI [72-77]. Of the mechanical measurements, apparent modulus and ultimate stress have been shown to decrease with age in the elderly using tibial bone in a mechanical compression test [78]. Although these studies do not address bisphosphonate treatment, they indirectly support the credibility of the methods used in this study to find significant correlations between treatment duration and bone microarchitecture and mechanical properties.

The apparent modulus can be described as a measure of the rigidity of the entire bone segment prior to the onset of plastic, or permanent, deformation. The apparent modulus as well as the effective modulus and estimated failure stress were isolated to the mechanical contributions of bone quantity and microarchitecture. This was because a constant tissue modulus was used throughout and other bone quality factors, such as microdamage and variations in mineralization, were not captured by the model used. Hence, bisphosphonate treatment initially was associated with an increase in the average rigidity due to the trabecular microarchitecture and volume, a maximum at approximately 7 years, and then a decline in the average rigidity.

Although the apparent modulus is limited to describing mechanical behavior prior to the yield point, it has been shown to be a predictor of bone strength [52]. This was

confirmed in the present study by the strong correlation between apparent modulus and failure stress ($R^2 = 0.98$). With this in mind, the apparent modulus and failure stress results provided insight into the trabecular bone's propensity to fracture. The contributions of bone quantity and microarchitecture to overall bone strength were greatest when apparent modulus and failure stress reached their maximum, approximately 7 years of bisphosphonate treatment. Beyond this duration of treatment, the load required to induce fracture decreased.

As a ratio of rigidity to percent bone volume, the effective modulus described how efficient the trabecular structure was in contributing to bone strength. While the measurement wasn't free from the influence of BV/TV, the influence of BV/TV was reduced, and the influence of trabecular structure was emphasized in the process. Trabecular bone was most efficient, or most rigid per bone fraction, at approximately 7 years of bisphosphonate treatment and then declined.

The trend of an initial positive association with bisphosphonate treatment followed by a negative association was evident in the relationship between treatment duration and BV/TV, SMI, CD, Tb.Th., and Tb.Sp. as well. The correlations taken together may provide insight into the mechanisms by which bone microarchitecture changes with duration of treatment. The response curve predicting the density of trabecular connections and the response curve relating trabecular separation to duration of treatment were similar in shape but the inverse of each other. Bisphosphonates may initially increase connectivity while concurrently reducing the space between trabeculae. Both improvements were reversed after extrema were reached at approximately 7 years of treatment. Trabecular thickness remained unchanged by bisphosphonate treatment, further suggesting that the variation in bone volume was driven by changes in trabecular connectivity.

Of the structural indices measured, SMI was the most unique being more deeply rooted in structure and less descriptive of bone quantity compared to the other indices. Analysis of SMI revealed that bisphosphonate treatment was initially associated with a

trend toward more plate-like bone followed by a reversal toward more rod-like bone. Previous studies have linked rod-like trabecular structures to osteoporosis and a decreased resistance to fracture [74, 79].

The uniqueness of the SMI measurement likely reduced the potential for collinearity with BV/TV that Tb.Sp. and CD appeared to show when modeled as predictors of the apparent modulus, effective modulus, and failure stress. BV/TV was the strongest single predictor of the biomechanical properties. This supported the attention placed on bone loss in diagnosing and monitoring osteoporosis. SMI, however, provided significant structural information independent of BV/TV in predicting the biomechanical properties. BV/TV and SMI together were significantly better at predicting the biomechanical properties than when considered separately. This further emphasizes the importance of piecing together multiple aspects of bone quantity and quality to provide a more complete picture of the bone's mechanical competency. Previous studies have shown that BV/TV, SMI, and even Tb.Sp. are each capable individual predictors of biomechanical properties [75, 80-82]. The best model to predict apparent modulus, effective modulus, and failure stress from microCT-derived structural indices included both BV/TV and SMI.

The initial positive effects on bone microarchitecture are in accord with the known mechanism of action of bisphosphonates. Bisphosphonates target osteoclasts to inhibit resorption and have been reported to promote bone formation as well [83]. This leads to a net gain in bone which can be observed by the increased BV/TV associated with initial treatment. Bone quality is improved along with bone quantity as the additional bone material is arranged to improve microarchitecture. This is evident in the increase in the averages for CD and SMI while Tb.Sp. decreased. The increase in effective modulus also indicates that the additional bone led to greater structural efficiency for subjects in the initial years of treatment.

Eventually, the balance in favor of formation is lost and beneficial effects of bisphosphonate treatment on quantity and microarchitecture plateau. Decreased

resorption likely leads to a decrease in formation based on the relationship between osteoblast and osteoclast activity. Another possibility is that continuous bisphosphonate uptake increases the drug concentration that reaches the osteoblasts. At a higher concentration, bisphosphonates shift from promoting osteoblastogenesis to causing apoptosis of both osteoclasts and osteoblasts [84]. Either scenario could explain why bisphosphonate treatment decreases bone turnover and does not continue to increase quantity and improve microarchitecture indefinitely.

Rather than a steady plateau, the results of this study showed eventual declines in bone quantity and microarchitecture with treatment duration. Without the ability to repair itself through remodeling, bone becomes susceptible to failure at reduced stresses from wear and fatigue. By inhibiting both bone resorption and formation, long-term bisphosphonate use may increase the potential for microdamage to go unrepaired. While microdamage was not considered in the present study, the consequences of accumulated microdamage may have been observed. The decline in BV/TV and CD accompanied by an increase in Tb.Sp. may reflect the loss of trabecular struts that have broken away due to the microdamage. Microcracks are known to grow and coalesce with continued repetitive loading [85]. Thus, bone mass isn't just lost; it is lost at key load-bearing structural junctions. The decreasing bone quantity and microarchitecture quality together lower the stress that the bone can withstand before fracturing.

Limitations

One of the limitations of this study was its cross-sectional nature. As such, each datum offered insight limited to the date that the biopsy was performed. Although some inferences could be assumed, the state of bone in each subject prior to or after the biopsy remained uncertain. It is not possible to definitively state that any or all of the subjects would have experienced the same initial positive outcomes followed by a decline after 7 years of treatment. To execute a longitudinal study of bisphosphonate treatment to the length captured in the present study does not appear feasible as it would require a biopsy from all subjects at each year of treatment. The design of this study best suited the resources available and still succeeded in meeting the study aims.

The biopsies collected and used for this study were from cores of either 3 or 4 mm diameter. According to the most widely accepted recommendations [60], the size of many of the biopsies used in this study were near the lower limit of the recommended five intratrabecular lengths. This standard for representation of the true in situ behavior has since been reexamined [71]. Their findings indicated that the apparent modulus calculated by FEA continued to increase as the diameter of the trabecular bone segment increased rather than converging on a constant modulus. Therefore, the apparent modulus values reported in this study cannot be assumed to be the accurate in situ value; rather, all presently reported values were undervalued according to the results of this prior study [71]. Going from independent cores to in situ, the apparent moduli of 2.81 mm and 3.96 mm vertebral cores increased 19.73% and 17.59%, respectively [71]. By limiting the range of specimen sizes, the relative differences between samples remained valid. Any error associated with the effect of specimen size in the form of side artifacts was corrected as recommended [86]. This was supported by the lack of significance of cross-sectional area as a predictor of any of the response variables. The values reported, therefore, are suitable as a comparative dataset; however, a larger specimen size would be desired to obtain a more accurate individual assessment of fracture risk.

Another potential limitation to this study was the use of a linear FEA rather than a nonlinear FEA. Although apparent modulus has been shown to correlate to bone strength and subsequently fracture resistance [53, 54], to definitively say that an increase or decrease in apparent modulus with bisphosphonate treatment is equivalent to an increase or decrease in fracture resistance with treatment assumes that the relationship between apparent modulus and fracture stress remains constant throughout the treatment duration. Until this assumption is validated, inferences about fracture with use of bisphosphonates must be interpreted with caution. Further mechanical testing examining the post-yield behavior of trabecular bone in response to bisphosphonate treatment is required. Such a study would also provide validation for a nonlinear analysis. Until this task is achieved, a nonlinear FEA would be no more reliable than this linear FEA study.

Finally, a greater sample size would increase the credibility of the study. Despite the large number of biopsies collected by the Kentucky Bone Registry, only 53 subjects met the established medical and biopsy quality criteria in order to be included in this study. This was less than the goal of 70 subjects set in the study design. It was especially hard to find subjects who had maintained continuous oral bisphosphonate treatment or greater than 12 years without having another medical reason for exclusion. The addition of samples in this range of treatment duration would instill greater confidence in the observation of the negative trends associated with these higher treatment durations. Given that the p-values for many of the significant relationships were less than 0.01, however, there is good reason to believe that the significant relationships would hold true with an increase in sample size.

Future Studies

To further assess the effects of long-term treatment, other aspects of bone quality must be accounted for in the model as well. A logical next step would be to add in aspects of trabecular bone tissue properties beginning with the tissue modulus specific to each bone segment. Nanoindentation is an established tool for determining the material properties of biological tissue [87]. Young's modulus of trabecular bone from nanoindentation of each biopsy could easily be coded into the FEA, and the combination of nanoindentation and FEA has been shown to be a robust method for predicting linear elastic mechanical properties [48].

Another option is the assignment of material properties based on microCT density measurements. An equation relating density to the tissue modulus could be used to assign the appropriate tissue modulus to each element of the mesh. With the material properties of each element as a product of the degree of mineralization, variations and defects in mineralization of the bone segment can be included in the FEA.

Microdamage is another aspect of bone quality that would benefit from inclusion in a study of long-term bisphosphonate treatment. Although the results weren't quite significant, an increase in markers of microdamage in subjects treated with alendronate

for a mean of 63.6 months compared to placebo has been observed [88]. Ideally, the finite element model would account for microdamage as well. Greater image resolution would be required for the presence of subject specific microcracks in the model.

Conclusion

       The present results show that beneficial contributions to trabecular failure strength, apparent modulus, and effective modulus peak at approximately 7 years of continuous bisphosphonate treatment then decline. Similar correlations were noted between duration of treatment and BV/TV, SMI, CD, and Tb.Sp. The relationships noted between bisphosphonate treatment duration and failure strength, apparent modulus, effective modulus, BV/TV, SMI, CD, and Tb.Sp. were independent of age and bone turnover. These findings confirmed that bisphosphonates provide short term benefits and contribute new information showing these benefits decline after reaching a maximum at approximately 7 years of treatment. These results suggest that bisphosphonates should not be prescribed without a defined endpoint, that other aspects of bone quality not in the present study may be declining with long-term treatment, and that the microCT derived measures of BV/TV, representing bone quantity, and SMI, representing bone microarchitecture, together adequately predict bone mechanical properties if FEA is unavailable.

APPENDIX: EXPLANATION OF VARIABLES
NOTE: Related variables are in red

- **Age:** Age of the patient on the date the biopsy was taken
- **Duration of Treatment in Years (Duration):** Total time that the patient had been continuously treated with bisphosphonates prior to date of biopsy
- **Threshold:** The lower grayscale threshold value used to dictate what is bone when creating a 3D segment from microCT images. Voxels with a grayscale intensity above the threshold are considered bone.

Input for FEA
- **Young's Modulus Trabecular Bone (Emat):** This is the stress per unit strain of the trabecular bone measured on the nanoscale and is in units of GigaPascals (GPa). An arbitrary value of 16 GPa was assigned to all the samples.

Direct Output of FEA
- **Reaction Force (Fy):** This the total reaction force along the axis of loading (y-axis) measured in Newtons (N).
- **Bone Volume (BV):** The total volume of the elements in the mesh which is the volume of bone material in the segment being analyzed. Measured in millimeters cubed (mm^3)
- **Segment Length (Length):** The length of the bone segment along the axis of loading (y-axis). Each biopsy was cut so that this value is a constant 4.00 mm.
- **Ultimate Force (Fult):** An estimate of the force along the y-axis required to cause overall failure of the biopsy segment. This is a calculation of the force at which 2% of the stressed bone volume reaches an equivalent strain of 0.007. Value reported in Newtons.

Direct Output of MicroCT 3D Evaluation
- **MicroCT Total Volume (μCT TV):** Total volume of the region of interest which is defined by contour lines drawn on each 2D slice. This includes both the bone and the porosity (bone marrow). Value reported in units of millimeters cubed.
- **MicroCT Length (μCT Length):** length along the y-axis of the biopsy segment analyzed in the 3D evaluation. Value reported in units of voxels where each voxel is 0.030 mm in length.
- **Connectivity Density (CD):** Estimate of the trabecular connectivity per unit volume. It is a measure of bone architecture and is reported in units of millimeters cubed.
- **Structure Model Index (SMI):** This is a gauge of whether the bone segment is more platelike or more rodlike in structure. Values range from 0 (parallel plates) to 3 (cylindrical rods). SMI is based on the curvature of the structure, so a value of 4 would correspond to a sphere, and a negative SMI value means that the surface is concave. Negative values are typically encountered when the BV/TV is high and cortical or subcortical bone is being measured.
- **Trabecular Thickness (Tb.Th.):** Average thickness of the trabeculae. Value reported in units of microns.

- **Trabecular Separation (Tb.Sp.):** Average thickness of the bone marrow. Value reported in units of microns.

Values Measured in Netfabb

- **Minimum Dimension (MinDim):** Measure of the shortest dimension of the bone biopsy segment. For whole biopsies, this would be the diameter of the bone cylinder. For cut biopsies, this value is the remaining portion of the diameter and is important in deciding whether or not the biopsy is useable. Value reported in millimeters.
- **Offset Angle (Offset):** The angle at which the bone segment for FEA differs from the segment analyzed in the microCT 3D evaluation. This is the angle of the biopsy going into the microCT slices and cannot be corrected for the 3D evaluation. Value reported in degrees.

Calculated Values

- **Cross-Sectional Area (Area):** The average area of the biopsy segment perpendicular to the axis of loading (y-axis). The following equation is used in the calculation:

$$Area = \frac{uCT\ TV}{uCT\ Length * 0.030/\cos(offset)}$$

- **BV/TV:** The ratio of the Bone Volume to the total volume of the biopsy segment. Since the microCT Total Volume is not of the exact same bone segment used in the FEA, the total volume is calculated as a product of the Length and the Cross-Sectional Area. The following equation is used in the calculation:

$$BV/TV = \frac{BV}{Area * Length}$$

- **Reaction Stress (Py):** This the total reaction stress along the axis of loading (y-axis) calculated by dividing the Reaction Force by the Cross-Sectional Area. Value is reported in units of MegaPascals (MPa).
- **Side Artifact Correction Factor:** This is a correction factor applied to the biomechanical variables because of connections lost around the perimeter of the bone segment. It is the ratio of the measured cross-sectional area to the true cross-sectional area. The true cross-sectional area is the measured cross-sectional area excluding the region of lost connections which has a thickness equal to half the trabecular separation.
- **Apparent Young's Modulus (Eapp):** This is a commonly reported measure of strength of the biopsy segment and is calculated by dividing the Reaction Stress by the strain applied to the biopsy segment and multiplying by the Side Artifact Correction Factor. The strain is a boundary condition of the FEA and is a constant arbitrary value of 0.01. Value is reported in units of GigaPascals (GPa).

- **Effective Young's Modulus (Eeff):** This value is an attempt to normalize the Apparent Young's Modulus values to the same BV/TV. Thus, it is a measurement of how efficiently the bone material is structured to contribute to the segment's rigidity. It is calculated by dividing the Apparent Young's Modulus by the BV/TV. Value is reported in units of GigaPascals (GPa).
- **Failure Stress (Pfail):** This is an estimate of the stress along the y-axis required to cause overall failure of the biopsy segment and is calculated by dividing the Ultimate Force by the Cross-Sectional Area and multiplying by the Side Artifact Correction Factor. Value is reported in units of MegaPascals (MPa).

REFERENCES

1. Carretta, R., S. Lorenzetti, and R. Muller, *Towards patient-specific material modeling of trabecular bone post-yield behavior.* Int J Numer Method Biomed Eng, 2013. **29**(2): p. 250-72.

2. Bartl, R., *Bisphosphonates in medical practice : actions, side effects, indications, strategies*. 2007, Berlin ; New York: Springer. xx, 265 p.

3. Currey, J.D., *The mechanical consequences of variation in the mineral content of bone.* J Biomech, 1969. **2**(1): p. 1-11.

4. Currey, J.D., *Physical characteristics affecting the tensile failure properties of compact bone.* J Biomech, 1990. **23**(8): p. 837-44.

5. van Rietbergen, B., et al., *A new method to determine trabecular bone elastic properties and loading using micromechanical finite-element models.* J Biomech, 1995. **28**(1): p. 69-81.

6. Fleisch, H., *Bisphosphonates in bone disease : from the laboratory to the patient*. 4th ed. 2000, San Diego: Academic Press. xii, 212 p.

7. Ott, S.M., *Histomorphometric measurements of bone turnover, mineralization, and volume.* Clin J Am Soc Nephrol, 2008. **3 Suppl 3**: p. S151-6.

8. Center, J.R., et al., *Mortality after all major types of osteoporotic fracture in men and women: an observational study.* Lancet, 1999. **353**(9156): p. 878-82.

9. Kanis, J.A., et al., *Excess mortality after hospitalisation for vertebral fracture.* Osteoporos Int, 2004. **15**(2): p. 108-12.

10. Abrahamsen, B., et al., *Excess mortality following hip fracture: a systematic epidemiological review.* Osteoporos Int, 2009. **20**(10): p. 1633-50.

11. *Assessment of fracture risk and its application to screening for postmenopausal osteoporosis. Report of a WHO Study Group.* World Health Organ Tech Rep Ser, 1994. **843**: p. 1-129.

12. *Diagnostic and therapeutic technology assessment. Measurement of bone density with dual-energy X-ray absorptiometry (DEXA).* JAMA, 1992. **267**(2): p. 286-8, 290-4.

13. Kanis, J.A., et al., *FRAX and the assessment of fracture probability in men and women from the UK.* Osteoporos Int, 2008. **19**(4): p. 385-97.

14. Riggs, B.L. and A.M. Parfitt, *Drugs used to treat osteoporosis: the critical need for a uniform nomenclature based on their action on bone remodeling.* J Bone Miner Res, 2005. **20**(2): p. 177-84.

15. Cooper, C., *Epidemiology of osteoporosis.* Osteoporos Int, 1999. **9 Suppl 2**: p. S2-8.

16. Nazarian, A., et al., *The interaction of microstructure and volume fraction in predicting failure in cancellous bone.* Bone, 2006. **39**(6): p. 1196-202.

17. *What is Osteoporosis?* [website] [cited 2014; Available from: http://nof.org/articles/7.

18. Nih Consensus Development Panel on Osteoporosis Prevention, D. and Therapy, *Osteoporosis prevention, diagnosis, and therapy.* JAMA, 2001. **285**(6): p. 785-95.

19. Rachner, T.D., S. Khosla, and L.C. Hofbauer, *Osteoporosis: now and the future.* Lancet, 2011. **377**(9773): p. 1276-87.

20. Hiligsmann, M., et al., *Lifetime absolute risk of hip and other osteoporotic fracture in Belgian women.* Bone, 2008. **43**(6): p. 991-4.

21. Kanis, J.A., et al., *Long-term risk of osteoporotic fracture in Malmo.* Osteoporos Int, 2000. **11**(8): p. 669-74.

22. Harvey, N., E. Dennison, and C. Cooper, *Osteoporosis: impact on health and economics.* Nat Rev Rheumatol, 2010. **6**(2): p. 99-105.

23. Lems, W.F. and P. Geusens, *Established and forthcoming drugs for the treatment of osteoporosis.* Curr Opin Rheumatol, 2014. **26**(3): p. 245-51.

24. Schmidt, G.A., et al., *Risks and benefits of long-term bisphosphonate therapy.* Am J Health Syst Pharm, 2010. **67**(12): p. 994-1001.

25. Chavassieux, P.M., et al., *Histomorphometric assessment of the long-term effects of alendronate on bone quality and remodeling in patients with osteoporosis.* J Clin Invest, 1997. **100**(6): p. 1475-80.

26. Liberman, U.A., et al., *Effect of oral alendronate on bone mineral density and the incidence of fractures in postmenopausal osteoporosis. The Alendronate Phase III Osteoporosis Treatment Study Group.* N Engl J Med, 1995. **333**(22): p. 1437-43.

27. Cummings, S.R., et al., *Effect of alendronate on risk of fracture in women with low bone density but without vertebral fractures: results from the Fracture Intervention Trial.* JAMA, 1998. **280**(24): p. 2077-82.

28. Harris, S.T., et al., *Effects of risedronate treatment on vertebral and nonvertebral fractures in women with postmenopausal osteoporosis: a randomized controlled trial. Vertebral Efficacy With Risedronate Therapy (VERT) Study Group.* JAMA, 1999. **282**(14): p. 1344-52.

29. Bilezikian, J.P., *Efficacy of bisphosphonates in reducing fracture risk in postmenopausal osteoporosis.* Am J Med, 2009. **122**(2 Suppl): p. S14-21.

30. Malluche, H.H., D.S. Porter, and D. Pienkowski, *Evaluating bone quality in patients with chronic kidney disease.* Nat Rev Nephrol, 2013. **9**(11): p. 671-80.

31. Boskey, A.L., L. Spevak, and R.S. Weinstein, *Spectroscopic markers of bone quality in alendronate-treated postmenopausal women.* Osteoporos Int, 2009. **20**(5): p. 793-800.

32. Allen, M.R. and D.B. Burr, *Three years of alendronate treatment results in similar levels of vertebral microdamage as after one year of treatment.* J Bone Miner Res, 2007. **22**(11): p. 1759-65.

33. Turner, C.H., *Biomechanics of bone: determinants of skeletal fragility and bone quality.* Osteoporos Int, 2002. **13**(2): p. 97-104.

34. Borah, B., et al., *Risedronate preserves bone architecture in postmenopausal women with osteoporosis as measured by three-dimensional microcomputed tomography.* Bone, 2004. **34**(4): p. 736-46.

35. Recker, R., et al., *Trabecular bone microarchitecture after alendronate treatment of osteoporotic women.* Curr Med Res Opin, 2005. **21**(2): p. 185-94.

36. Lewiecki, E.M., et al., *Once-monthly oral ibandronate improves biomechanical determinants of bone strength in women with postmenopausal osteoporosis.* J Clin Endocrinol Metab, 2009. **94**(1): p. 171-80.

37. Burghardt, A.J., et al., *A longitudinal HR-pQCT study of alendronate treatment in postmenopausal women with low bone density: Relations among density, cortical and trabecular microarchitecture, biomechanics, and bone turnover.* J Bone Miner Res, 2010. **25**(12): p. 2558-71.

38. Black, D.M., et al., *Effects of continuing or stopping alendronate after 5 years of treatment: the Fracture Intervention Trial Long-term Extension (FLEX): a randomized trial.* JAMA, 2006. **296**(24): p. 2927-38.

39. Recker, R.R., et al., *Safety of bisphosphonates in the treatment of osteoporosis.* Am J Med, 2009. **122**(2 Suppl): p. S22-32.

40. Shane, E., et al., *Atypical subtrochanteric and diaphyseal femoral fractures: report of a task force of the American Society for Bone and Mineral Research.* J Bone Miner Res, 2010. **25**(11): p. 2267-94.

41. Watts, N.B. and D.L. Diab, *Long-term use of bisphosphonates in osteoporosis.* J Clin Endocrinol Metab, 2010. **95**(4): p. 1555-65.

42. Whitaker, M., et al., *Bisphosphonates for osteoporosis--where do we go from here?* N Engl J Med, 2012. **366**(22): p. 2048-51.

43. Isaksson, H., et al., *Structural parameters of normal and osteoporotic human trabecular bone are affected differently by microCT image resolution.* Osteoporos Int, 2011. **22**(1): p. 167-77.

44. Muller, R., et al., *Morphometric analysis of human bone biopsies: a quantitative structural comparison of histological sections and micro-computed tomography.* Bone, 1998. **23**(1): p. 59-66.

45. Chappard, D., et al., *Comparison insight bone measurements by histomorphometry and microCT.* J Bone Miner Res, 2005. **20**(7): p. 1177-84.

46. Tamminen, I.S., et al., *Reproducibility and agreement of micro-CT and histomorphometry in human trabecular bone with different metabolic status.* J Bone Miner Metab, 2011. **29**(4): p. 442-8.

47. Pugh, J.W., R.M. Rose, and E.L. Radin, *A structural model for the mechanical behavior of trabecular bone.* J Biomech, 1973. **6**(6): p. 657-70.

48. Chevalier, Y., et al., *Validation of a voxel-based FE method for prediction of the uniaxial apparent modulus of human trabecular bone using macroscopic mechanical tests and nanoindentation.* J Biomech, 2007. **40**(15): p. 3333-40.

49. Bevill, G., et al., *The influence of boundary conditions and loading mode on high-resolution finite element-computed trabecular tissue properties.* Bone, 2009. **44**(4): p. 573-8.

50. Burkhart, T.A., D.M. Andrews, and C.E. Dunning, *Finite element modeling mesh quality, energy balance and validation methods: a review with recommendations associated with the modeling of bone tissue.* J Biomech, 2013. **46**(9): p. 1477-88.

51. Keaveny, T.M., et al., *Trabecular bone exhibits fully linear elastic behavior and yields at low strains.* J Biomech, 1994. **27**(9): p. 1127-36.

52. Bevill, G. and T.M. Keaveny, *Trabecular bone strength predictions using finite element analysis of micro-scale images at limited spatial resolution.* Bone, 2009. **44**(4): p. 579-84.

53. Macneil, J.A. and S.K. Boyd, *Bone strength at the distal radius can be estimated from high-resolution peripheral quantitative computed tomography and the finite element method.* Bone, 2008. **42**(6): p. 1203-13.

54. Pistoia, W., et al., *Estimation of distal radius failure load with micro-finite element analysis models based on three-dimensional peripheral quantitative computed tomography images.* Bone, 2002. **30**(6): p. 842-8.

55. Cohen, A., et al., *Abnormal bone microarchitecture and evidence of osteoblast dysfunction in premenopausal women with idiopathic osteoporosis.* J Clin Endocrinol Metab, 2011. **96**(10): p. 3095-105.

56. Harrison, N.M., et al., *Failure modelling of trabecular bone using a non-linear combined damage and fracture voxel finite element approach.* Biomech Model Mechanobiol, 2013. **12**(2): p. 225-41.

57. De, S., F. Guilak, and M.R.K. Mofrad, *Computational modeling in biomechanics*. 2010, Dordrecht ; New York: Springer. viii, 581 p.

58. Wilkerson, L.T., *Finite Element Analysis of Cancellous Bone*, in *Mechanical Engineering*. 2012, University of Kentucky: Theses and Dissertations.

59. Malluche, H.H., et al., *Differences in bone quality in low- and high-turnover renal osteodystrophy.* J Am Soc Nephrol, 2012. **23**(3): p. 525-32.

60. Harrigan, T.P., et al., *Limitations of the continuum assumption in cancellous bone.* J Biomech, 1988. **21**(4): p. 269-75.

61. Peters, T., *CT image reconstruction.*

62. Ruegsegger, P., B. Koller, and R. Muller, *A microtomographic system for the nondestructive evaluation of bone architecture.* Calcif Tissue Int, 1996. **58**(1): p. 24-9.

63. Waarsing, J.H., J.S. Day, and H. Weinans, *An improved segmentation method for in vivo microCT imaging.* J Bone Miner Res, 2004. **19**(10): p. 1640-50.

64. Ding, M., A. Odgaard, and I. Hvid, *Accuracy of cancellous bone volume fraction measured by micro-CT scanning.* J Biomech, 1999. **32**(3): p. 323-6.

65. Klingner, B.M. and J.R. Shewchuk. *Aggressive tetrahedral mesh improvement*. in *Proceedings of the 16th international meshing roundtable*. 2008. Springer.

66. Lewis, G. and J.S. Nyman, *The use of nanoindentation for characterizing the properties of mineralized hard tissues: state-of-the art review.* J Biomed Mater Res B Appl Biomater, 2008. **87**(1): p. 286-301.

67. Un, K., G. Bevill, and T.M. Keaveny, *The effects of side-artifacts on the elastic modulus of trabecular bone.* J Biomech, 2006. **39**(11): p. 1955-63.

68. Rosner, B., *Fundamentals of biostatistics*. 7th ed. 2011, Boston: Brooks/Cole, Cengage Learning. xvii, 859 p.

69. Dell, R.M., et al., *Incidence of atypical nontraumatic diaphyseal fractures of the femur.* J Bone Miner Res, 2012. **27**(12): p. 2544-50.

70. Meier, R.P., et al., *Increasing occurrence of atypical femoral fractures associated with bisphosphonate use.* Arch Intern Med, 2012. **172**(12): p. 930-6.

71. Harrison, N.M. and P.E. McHugh, *Comparison of trabecular bone behavior in core and whole bone samples using high-resolution modeling of a vertebral body.* Biomech Model Mechanobiol, 2010. **9**(4): p. 469-80.

72. Thomsen, J.S., E.N. Ebbesen, and L. Mosekilde, *Static histomorphometry of human iliac crest and vertebral trabecular bone: a comparative study.* Bone, 2002. **30**(1): p. 267-74.

73. Thomsen, J.S., E.N. Ebbesen, and L. Mosekilde, *Relationships between static histomorphometry and bone strength measurements in human iliac crest bone biopsies.* Bone, 1998. **22**(2): p. 153-63.

74. Ding, M. and I. Hvid, *Quantification of age-related changes in the structure model type and trabecular thickness of human tibial cancellous bone.* Bone, 2000. **26**(3): p. 291-5.

75. Link, T.M., et al., *Structure analysis of high resolution magnetic resonance imaging of the proximal femur: in vitro correlation with biomechanical strength and BMD.* Calcif Tissue Int, 2003. **72**(2): p. 156-65.

76. Boutroy, S., et al., *In vivo assessment of trabecular bone microarchitecture by high-resolution peripheral quantitative computed tomography.* J Clin Endocrinol Metab, 2005. **90**(12): p. 6508-15.

77. Khosla, S., et al., *Effects of sex and age on bone microstructure at the ultradistal radius: a population-based noninvasive in vivo assessment.* J Bone Miner Res, 2006. **21**(1): p. 124-31.

78. Ding, M., et al., *Age variations in the properties of human tibial trabecular bone.* J Bone Joint Surg Br, 1997. **79**(6): p. 995-1002.

79. Karim, L. and D. Vashishth, *Role of trabecular microarchitecture in the formation, accumulation, and morphology of microdamage in human cancellous bone.* J Orthop Res, 2011. **29**(11): p. 1739-44.

80. Goulet, R.W., et al., *The relationship between the structural and orthogonal compressive properties of trabecular bone.* J Biomech, 1994. **27**(4): p. 375-89.

81. Thomsen, J.S., E.N. Ebbesen, and L. Mosekilde, *Predicting human vertebral bone strength by vertebral static histomorphometry.* Bone, 2002. **30**(3): p. 502-8.

82. Mittra, E., et al., *Evaluation of trabecular mechanical and microstructural properties in human calcaneal bone of advanced age using mechanical testing, microCT, and DXA.* J Biomech, 2008. **41**(2): p. 368-75.

83. Bellido, T. and L.I. Plotkin, *Novel actions of bisphosphonates in bone: preservation of osteoblast and osteocyte viability.* Bone, 2011. **49**(1): p. 50-5.

84. Idris, A.I., et al., *Aminobisphosphonates cause osteoblast apoptosis and inhibit bone nodule formation in vitro.* Calcif Tissue Int, 2008. **82**(3): p. 191-201.

85. Favus, M.J. and American Society for Bone and Mineral Research., *Primer on the metabolic bone diseases and disorders of mineral metabolism*. 5th ed. 2003, Washington, DC: American Society for Bone and Mineral Research. p.

86. Bevill, G., S.K. Easley, and T.M. Keaveny, *Side-artifact errors in yield strength and elastic modulus for human trabecular bone and their dependence on bone volume fraction and anatomic site.* J Biomech, 2007. **40**(15): p. 3381-8.

87. Oliver, W.C. and G.M. Pharr, *An improved technique for determining hardness and elastic modulus using load displacement sensing indentation experiments.* J Mater Res, 1992. **7**(6): p. 1564-1583.

88. Stepan, J.J., et al., *Low bone mineral density is associated with bone microdamage accumulation in postmenopausal women with osteoporosis.* Bone, 2007. **41**(3): p. 378-85.

VITA

Jonathan Joseph Ward was born in North East, PA, and graduated *cum laude* with a B.E. in Mechanical Engineering from Grove City College in Grove City, PA in 2011. While at the University of Kentucky, he was awarded the USEC Fellowship in 2012 and served as a research assistant.